processes

MDPI

Article

Investigation on the Separation Performance and Multiparameter Optimization of Decanter Centrifuges

Xiang Kang, Liuxi Cai *, Yun Li, Xiufeng Gao and Guangqian Bai

School of Chemical Engineering and Technology, Xi'an Jiaotong University, Xianning West Road No. 28, Xi'an 710049, China; kangxiang985@stu.xjtu.edu.cn (X.K.); yunli@mail.xjtu.edu.cn (Y.L.); xfgao@mail.xjtu.edu.cn (X.G.); dabai721@yeah.net (G.B.)

* Correspondence: liuxicai@xjtu.edu.cn; Tel./Fax: +86-29-8896-8954

Abstract: Decanter centrifuges are widely used for solid–liquid separation. Although parameter analysis for decanter centrifuges was performed by numerical simulation in previous studies, some structural parameters are rarely mentioned and investigated. At the same time, the results obtained by the single-parameter analysis in previous studies are difficult to truly realize the comprehensive performance optimization of decanter centrifuges. In this paper, the influences of the window structure and bowl–conveyor gap on the separation performance are systematically analyzed with the employment of a numerical computation method. The results show that the increase in the window angle and window height will accelerate the flow of the upper layer, while the increase in the bowl–conveyor gap may make particles flow through it directly and further form a solid retention zone. Both of the structural changes will lead to deterioration of the separation performance. On the basis of numerical simulation analysis, a genetic algorithm-based method for multiparameter optimization is proposed in this paper. Parameter optimization shows that bowl speed and feed flow rate have the most significant effects on the separation performance and power consumption. Compared with the minimal specific power in the first generation, the optimized specific power is reduced by 15.7%, and the cake solid content merely decreases by 0.044%.

Keywords: decanter centrifuge; separation performance; structural optimization; orthogonal test; genetic algorithm

Citation: Kang, X.; Cai, L.; Li, Y.; Gao, X.; Bai, G. Investigation on the Separation Performance and Multiparameter Optimization of Decanter Centrifuges. *Processes* **2022**, *10*, 1284. https://doi.org/10.3390/pr10071284

Academic Editors: Máté Petrik, Gábor L. Szepesi and Zoltán Szamosi

Received: 9 May 2022
Accepted: 27 June 2022
Published: 29 June 2022

1. Introduction

Decanter centrifuges have been widely applied in industries such as chemical engineering, pharmaceuticals, food, and water treatment. They have the advantages of high security, high reliability, continuous operation, low labor cost, and a small footprint. A mixture of density differences in phases such as liquid–solid or liquid–liquid, can be handled by centrifugal sedimentation [1]. Due to their unreasonable structural design, decanter centrifuges often have problems such as low separation efficiency and high power consumption during service [2]. Therefore, it is of great significance to carry out the separation performance prediction and structural optimization design of the decanter centrifuge for its efficient and economical operation.

It is difficult to measure the internal flow field of decanter centrifuges accurately, owing to their high-speed conditions [3]. However, the flow field characteristics can be obtained with the rapid development of the computational fluid dynamics (CFD) simulation. Based on the Euler multiphase flow model, renormalization group (RNG) turbulence model, and multiple reference system (MRF) approach, the pressure and velocity distributions were obtained [4,5]. The results show that the static pressure gradually increases along the radial direction, reaching the maximum at the inner wall of the bowl, and it has a decreasing trend along the axial direction. Dong et al. [6] analyzed the application of seven typical turbulence models for the simulation of decanter centrifuges, and their results show that the RNG k-ε model is in good agreement with

the literature value. Zhu et al. [7] explored the flow field in a novel three-phase decanter centrifuge with a vertical board and annular separation plate. The crystal particle size distribution in a salt precipitation flow field was investigated by using a coupled CFD-PBM approach [8,9]. Romaní et al. [10] analyzed the multiphase flow of water, air, and particles in a cylindrical solid bowl centrifuge by using a coupled CFD-DEM approach. They found that the sediment built at a higher angular velocity and normal pressure acting on the bowl wall is flatter and extends along the wall rather than in the radial direction. Menesklou et al. [11] presented a physically based computational model to predict the dynamic behavior of decanter centrifuges. Their method considers settling behavior, cake consolidation, and sediment transport by means of material functions. Gleiss et al. [12] established a mathematical model of the separation process in countercurrent decanter centrifuges, which takes into account the influence of the sediment build-up and the flow pattern. Hammerich et al. [13] proposed a method to simulate the equilibrium and transient consolidation of particulate networks in one dimension. It is based on the Eulerian approach for approximation of the volume fraction of the dispersed phase, without solving any additional partial differential equations.

The results from some numerical simulation studies show that suspension properties, structural parameters, and operating conditions have impacts on the flow field of decanter centrifuges. Zhu et al. [14] proved that the separation efficiency improved as the feed content increased. Yuan et al. [15] demonstrated that a longer conical section can improve the cake solid content, while a longer cylindrical section and larger pool depth can improve centrate clarification. Furthermore, the effects of the L/D (length to diameter) ratio, viscosity, and particle diameter were analyzed by applying the RSM model and DPM model [2,16]. These studies of decanter centrifuges focus on the pressure and velocity field, as well as the effects of the L/D ratio, bowl speed, solid particle size, etc. However, there are other structural parameters (window structure, bowl–conveyor gap, etc.) that also have impacts on the separation performance but are rarely mentioned in the current research.

Although the above studies have studied the structure and separation performance of the decanter centrifuge, the studies all take the separation performance as a single objective to optimize the decanter centrifuge structure, ignoring the impact of structural changes on the power consumption of the decanter centrifuge. This kind of single-parameter study makes it difficult to truly realize scheme optimization for decanter centrifuges. In fact, better separation results may lead to higher power consumption, which means that separation performance and centrifuge power consumption (cost) need to be considered at the same time. Thus, multi-objective optimization for decanter centrifuges is indispensable.

In this paper, the flow field of decanter centrifuges as well as the impacts of window structure and bowl–conveyor gap on the separation performance are investigated by applying the CFD method, coupled with the RNG turbulence model and MRF model. Based on the simulation results, a genetic algorithm-based method for optimizing the comprehensive performance of decanter centrifuges is proposed, and regression models of cake solid content and specific power are obtained by orthogonal numerical test results, which are treated as the objective function for optimization. After systematic structural and parameter optimization, a decanter centrifuge structure with higher separation performance and optimized specific power is finally obtained. The results and the optimization method proposed in this paper can provide a technical basis for the design of an efficient and economical decanter centrifuge.

2. Numerical Methods

2.1. Model Description

A decanter centrifuge is mainly composed of a bowl, screw conveyor, feed tube, feed accelerator, weir plate, etc. As shown in Figure 1, the suspension flows through the feed tube and enters the rotary bowl after being accelerated by the feed accelerator. The screw

conveyor pushes the cake (sediment) to the outlet at the end of the conical section; the centrate flows to the opposite end of the bowl. Thus, the suspension can be separated. In this paper, the fluid domain model for simulation is built based on a company's LW520 decanter centrifuge. The structural parameters are shown in Table 1, and a few notes in terms of model building are as follows.

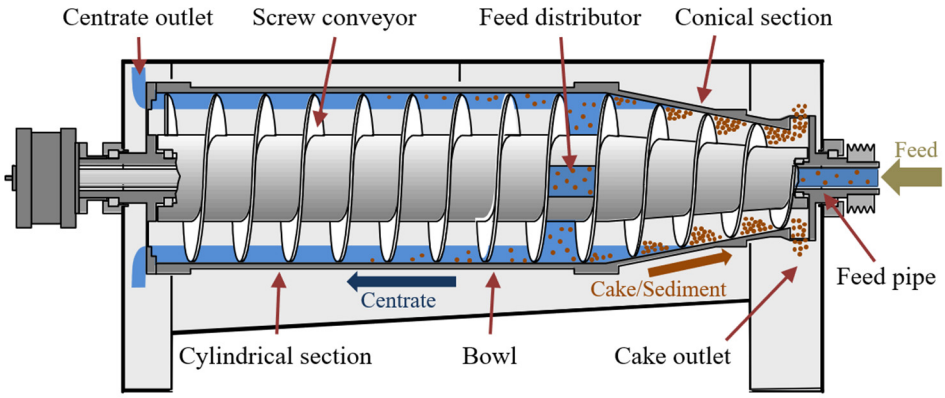

Figure 1. Schematic diagram of decanter centrifuges.

Table 1. Structural parameters of the LW520 decanter centrifuge.

Parameter	Value
Bowl diameter D (mm)	520
Cylindrical section length l_1 (mm)	870
Conical section length l_2 (mm)	690
Pool depth h (mm)	90
Half conical angle β (°)	9
Helical pitch S (mm)	130
Helical direction	Left

Assume that the space inside the bowl is filled with suspension. The air inside the bowl may have an impact on the flow field. However, the relative deviations of the cake solid content and solid recovery are acceptable, which has been proven by the results of simulations and experiments [14]. A rotating domain consists of the bowl, conveyor shaft, and feed accelerator, while the feed tube can be considered a stationary domain, taking into account the pre-acceleration impact.

A geometric model is set up by the 3D modeling software Creo. First, the structural parts, such as bowl, screw conveyor, and feed tube, are modeled. Then, the fluid domain is obtained by Boolean operation.

Ansys/ICEM and the multi-area meshing method are used to disperse the fluid domain. The region near the walls of the bowl, screw conveyor, and shaft are refined according to the requirement from the turbulence model. The grid independence test result is shown in Figure 2. It can be seen that, when the number of grids exceeds 590,000, the variation of the key parameter cake solid content is less than 0.4%. Considering the calculation accuracy and cost, the mesh number of the model under different calculation conditions is about 600,000. To demonstrate the flow field characteristics, the flow field is observed and analyzed by contours of the sections at equal intervals along the axial direction, as shown in Figure 3.

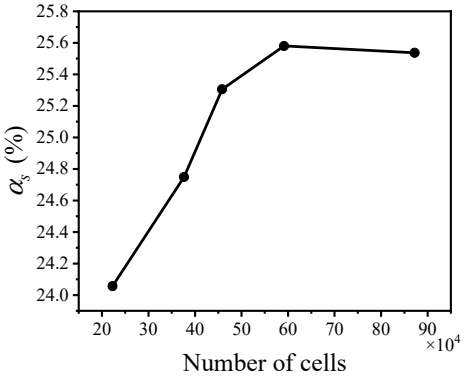

Figure 2. Correlation between the number of grids and the cake solid content.

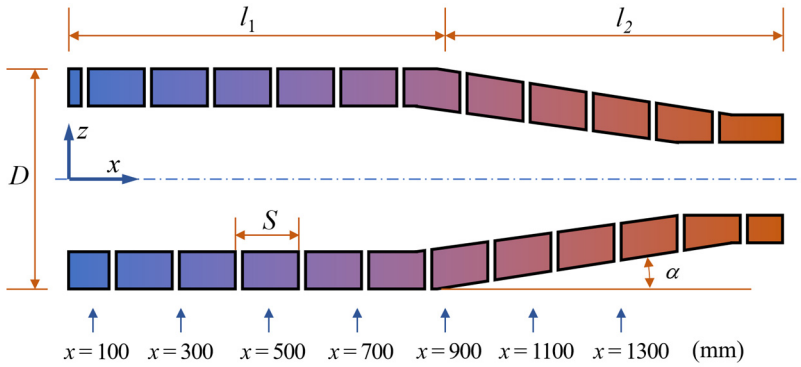

Figure 3. Positions for flow field observation.

2.2. Multiphase Flow Model and Conservation Equations

There are several multiphase flow models, such as the volume of fluid (VOF), mixture, Eulerian models, etc. For stratified or free-surface flows, the VOF model is appropriate; for flows in which the phases mix or separate and the dispersed-phase volume fractions exceed 10%, the mixture and Eulerian models are acceptable. In addition, the mixture model may be preferable if there is a wide distribution of dispersed phases. If the dispersed phases are concentrated in only portions of the domain, the Eulerian model should be used instead.

For decanter centrifuges, the solid phase, as the dispersed phase, is concentrated near the cake outlet, since the sediment is pushed to the front end by the screw conveyor. Thus, the Eulerian two-phase model is selected in this paper [5], and the volume fraction equation is

$$\sum_{q=1}^{n} \alpha_q = 1 \tag{1}$$

where, α_q is the volume fraction of phase q.

Each of the two phases satisfies the continuity equation.

$$\frac{\partial}{\partial t}(\alpha_q \rho_q) + \nabla \cdot (\alpha_q \rho_q v_q) = \sum_{p=1}^{n} (\dot{m}_{pq} - \dot{m}_{qp}) + S_q \tag{2}$$

where v_q is the velocity of phase q, $\dot{m}_{pq}$ is the mass transfer from phase p to phase q, and $\dot{m}_{qp}$ is the mass transfer from phase q to phase p. S_q is the source term and its default value is zero.

The equation of momentum conservation is as follows.

$$\begin{aligned} &\tfrac{\partial}{\partial t}(\alpha_l \rho_l v_l) + \nabla \cdot (\alpha_l \rho_l v_l v_l) = -\alpha_l \nabla p_l + \nabla \cdot \tau_l + \alpha_l \rho_l g \\ &+ \sum_{s=1}^{n} \left(K_{sl}(v_s - v_l) + \dot{m}_{sl} v_{sl} - \dot{m}_{ls} v_{ls} \right) + \left(F_l + F_{lift,l} + F_{wl,l} + F_{vm,l} + F_{td,l} \right) \end{aligned} \tag{3}$$

$$\begin{aligned}&\frac{\partial}{\partial t}(\alpha_s\rho_s v_s)+\nabla\cdot(\alpha_s\rho_s v_s v_s)=-\alpha_s\nabla p_s+\nabla\cdot\tau_s+\alpha_s\rho_s g\\&+\sum_{l=1}^{n}\left(K_{ls}(v_l-v_s)+\dot{m}_{ls}v_{ls}-\dot{m}_{sl}v_{sl}\right)+\left(F_s+F_{lift,s}+F_{vm,s}+F_{td,s}\right)\end{aligned}\tag{4}$$

where g is the gravitational acceleration. F_q is the external force, $F_{lift,q}$ is the lift force, $F_{vm,q}$ is the virtual mass force, $F_{td,q}$ is the turbulent dispersion force, and $F_{wl,q}$ is the wall lubrication force. Since the main forces on the particles are centrifugal force and drag force, the effect of other forces can be neglected. K_{ls} is the interphase momentum exchange coefficient and the drag force is calculated using the Gidaspow model [17].

When $\alpha_l > 0.8$,

$$K_{ls}=\frac{3}{4}C_D\frac{\alpha_s\rho_l|v_s-v_l|}{d_s}\tag{5}$$

$$C_D=\alpha_l{}^{-1.65}\max\left\{\frac{24}{\alpha_l Re_s}\left[1+0.15(\alpha_l Re_s)^{0.687}\right],0.44\right\}\tag{6}$$

When $\alpha_l \leq 0.8$,

$$K_{ls}=150\frac{\alpha_s(1-\alpha_l)\mu_l}{\alpha_l {d_s}^2}+1.75\frac{\rho_l\alpha_s|v_s-v_l|}{d_s}\tag{7}$$

where Re_s is the relative Reynolds coefficient, μ_l is the dynamic viscosity of the liquid phase, and d_s is the solid particle diameter.

Compared with the standard k-ε model, the effect of swirl on turbulence is included in the RNG k-ε model [18], enhancing the accuracy for swirling flows. While the standard k-ε model is a high-Reynolds-number model, the RNG theory provides an analytically derived differential formula for effective viscosity that accounts for low-Reynolds-number effects. Therefore, the RNG k-ε model is selected for the turbulence model in this paper, and the form of the turbulent kinetic energy and dissipation rate equations are given in Equations (8) and (9).

$$\begin{aligned}&\frac{\partial}{\partial t}(\rho k)+\frac{\partial}{\partial x_i}(\rho k u_i)=\frac{\partial}{\partial x_j}(\alpha_k\mu_{eff}\frac{\partial k}{\partial x_j})\\&+G_k+G_b-\rho\varepsilon-Y_M+S_k\end{aligned}\tag{8}$$

$$\begin{aligned}&\frac{\partial}{\partial t}(\rho\varepsilon)+\frac{\partial}{\partial x_i}(\rho\varepsilon u_i)=\frac{\partial}{\partial x_j}(\alpha_\varepsilon\mu_{eff}\frac{\partial\varepsilon}{\partial x_j})\\&+C_{1\varepsilon}\frac{\varepsilon}{k}(G_k+C_{3\varepsilon}G_b)-C_{2\varepsilon}\rho\frac{\varepsilon^2}{k}-R_\varepsilon+S_\varepsilon\end{aligned}\tag{9}$$

where G_k represents the generation of turbulence kinetic energy due to the mean velocity gradients. G_b is the generation of turbulence kinetic energy due to buoyancy. Y_M represents the contribution of the fluctuating dilatation in compressible turbulence to the overall dissipation rate. The quantities α_k and α_ε are the inverse effective Prandtl numbers for k and ε, respectively. S_k and S_ε are user-defined source terms.

2.3. Boundary Conditions

The flow field is solved by using FLUENT software. A velocity inlet boundary condition is adopted at the feed tube inlet, which is defined by setting the turbulence intensity and the hydraulic diameter. The velocity is 1.2 m/s and is perpendicular to the inlet plane. The solid phase is talcum powder, and its density is 2600 kg/m^3. The liquid phase is water, and its density is 998.2 kg/m^3. Both can be regarded as incompressible fluids. The feed solid content is 20%, and the solid particle diameter is 20 μm. Since the flow velocity and pressure at the cake and contrate outlets are unknown, it is assumed that the normal gradient of all flow parameters at the outlet, except pressure, is zero, i.e., outflow boundary conditions are used at the outlets. No-slip conditions are used for all walls.

The MRF model is used in this paper. The moving reference frame zone rotates at 3000 r/min. The walls of the screw conveyor are defined as moving walls, rotating in the same direction at a differential speed of 50 r/min. The intersection of the moving and stationary reference frame zone is defined as an interface boundary condition.

3. Multiparameter Optimization Method

To optimize the comprehensive performance of decanter centrifuges, it is necessary to consider the effects of several main parameters simultaneously. A genetic algorithm-based method is proposed in this section. Compared with the steepest ascent method, it can handle a complex objective function and avoid being trapped in a local optimal solution.

The optimization objective of the comprehensive performance consists of power consumption and separation effect. Mathematical models can be obtained from the simulation results of the designed schemes. The simulation method can avoid manufacturing decanter centrifuges of different sizes, which is effective and economical. Orthogonal numerical tests are adopted in this paper. Compared with the overall tests, they can reduce the number of tests and shorten the period for numerical calculation. Moreover, significant levels of the parameters can be explored by this method.

3.1. Performance Evaluation Metrics

The separation performance and power consumption of decanter centrifuges are both subject to multiple parameters. Their significance levels are explored based on orthogonal numerical tests.

Decanter centrifuges are designed for removing liquid in the suspension and dewatering the cake. Thus, the cake solid content can be used to evaluate the separation performance. In addition, the power consumption affects the operating cost. Since the inlet flow rate and the cake solid content are different in each case, the definition of specific power, $\overline{P}$, is proposed as a metric. It represents the energy required per unit volume of liquid removal.

$$\overline{P} = P/Q_{rem} \tag{10}$$

where P is the power required under stable operating conditions. Q_{rem} is the volume flow rate of the liquid removal, which equals the flow rate of the liquid phase at the centrate outlet:

$$Q_{rem} = Q_{cen}\alpha_{l,cen} \tag{11}$$

The liquid phase in the feed is eventually discharged from two outlets. The continuity equations for decanter centrifuges can be expressed as

$$Q_{feed} = Q_{cake} + Q_{cen} \tag{12}$$

$$Q_{feed}\alpha_{l,feed} = Q_{cake}\alpha_{l,cake} + Q_{cen}\alpha_{l,cen} \tag{13}$$

where Q_{feed}, Q_{cake}, and Q_{cen} are the flow rates of the feed, cake, and centrate, respectively. $\alpha_{l,feed}$, $\alpha_{l,cake}$, and $\alpha_{l,cen}$ are the liquid contents of feed, cake, and centrate, respectively. Solving Equations (10)–(13) for the specific power $\overline{P}$ gives

$$\overline{P} = \frac{P(1-\alpha_{l,cake})}{Q\left(\alpha_{l,feed}-\alpha_{l,cake}\right)} \tag{14}$$

The mathematical model of power consumption has been explored in the relevant research [19]. It consists of feed acceleration, cake transport, windage, and transmission losses. The power required for feed acceleration and cake transport accounts for the major part. The feed acceleration power, P_A, is mainly used for the feed kinetic energy increase and the viscous losses during acceleration, which can be expressed as:

$$P_A = \omega^2\left(\dot{m}_s {R_s}^2 + \dot{m}_l {R_l}^2\right) \tag{15}$$

where ω is the angular velocity of the bowl, $\dot{m}$ is the mass flow rate of the feed, R is the bowl radius at the cylindrical section, $\dot{m}_s$ is the mass flow rate at the cake outlet, $\dot{m}_l$ is the

mass flow rate at the centrate outlet, R_s is the bowl radius at the cake outlet, and R_l is the weir radius at the centrate outlet.

The decanter centrifuge is divided into four zones according to the bowl structure and whether the cake emerges from the pool [20]. The cake transport power can be obtained by calculating the power that each zone requires and summing them. In each zone, the internal flow field is divided into micro elements along the spiral line, and the power of each element is calculated as follows.

$$\delta\overline{P}_T = \frac{\overline{R}^2_{avx}(1 - S/\overline{\rho})(\tan\beta + \mu_3)(1 + \mu_1 \cot\alpha)(1 + \varepsilon_{cor})}{(1 - \mu_1 \tan\alpha)(1 - \mu_3 \tan\beta) - \mu_2 \sec\beta(\tan\alpha + \mu_1)}\delta\overline{x} \tag{16}$$

where, $\delta\overline{P}_T$ is the dimensionless power consumed by each element, $\overline{R}_{avx}$ is the dimensionless radius of the cake pressure center, S is the saturation, and $\overline{\rho}$ is the solid relative density. β is the half conical angle of the bowl, and α is the helix lift angle. ε_{cor} is the contribution of the Coriolis force to the power, which can be neglected. The friction coefficients among the cake, the screw conveyor, and the central shaft are μ_1, μ_2, and μ_3, respectively. $\delta\overline{x}$ is the dimensionless length of the element.

3.2. Orthogonal Numerical Test Design

An orthogonal test is a method for researching a target that has multiple factors and levels. Factors are arranged in an orthogonal table. Each level or factor appears an equal number of times. It is effective for product development and industrial engineering and has been successfully applied in numerous research areas [21].

The specific power and cake solid content are used as the metrics for the orthogonal numerical tests in this paper. First, the cake solid content and solid recovery are obtained by numerical simulation. Then, the specific power for each scheme is calculated by the method mentioned above. Finally, the significance levels of these parameters are analyzed. The sum of the feed acceleration power and cake transport power equals the aggregate power. The three friction coefficients are taken as 0.1, and the power used for transporting the cake at the cylindrical section is considered.

For a specific suspension, the solid density, particle size, viscosity, feed solid content, and other parameters are determined by a practical process. They are difficult to adjust or improve. However, structural parameters such as the L/D ratio and half conical angle, as well as operating parameters such as the bowl speed and flow rate can be adjusted. Therefore, they are used as orthogonal test parameters.

In this paper, based on a decanter centrifuge with a bowl diameter of 520 mm, five main parameters are investigated: L/D ratio δ, bowl speed n_b, differential speed n_d, flow rate Q, and half conical angle β. A sixth empty column is added as an error column. Table 2 shows the factors and levels of the orthogonal tests. Five levels, six factors, and 25 schemes are arranged. A standard orthogonal table, $L_{25}(5^6)$, is used. The geometric model must be rebuilt when the L/D ratio or half conical angle changes. The boundary conditions must be altered when the differential speed, bowl speed, or flow rate changes.

Table 2. Factors and levels of the orthogonal numerical tests.

Level	δ	n_b (r/min)	n_d (r/min)	Q (m^3/h)	β (°)
1	2.7	2000	5	3	7
2	2.9	2500	10	4	8
3	3.0	3000	15	5	10
4	3.1	3500	20	6	11
5	3.3	4000	25	7	12

3.3. Objective and Process of Genetic Algorithms

Three main aspects are considered to evaluate the comprehensive performance of a decanter centrifuge. The first is whether the separation effect can achieve the process

requirements. The second is how to further reduce the power consumption and operating cost. The third is how to lower the manufacturing cost, such as reducing the L/D ratio. Thus, the minimum specific power and the L/D ratio are treated as the optimization objectives of the comprehensive performance, under the condition of reaching the required cake solid content. The objective functions are described by:

$$\begin{cases} \min f(x) \\ \min x_1 \\ s.t. \quad g(x) \geq \alpha_{s,\min},\ 2.7 \leq x_1 \leq 3.3, \\ \qquad 2000 \leq x_2 \leq 4000,\ 5 \leq x_3 \leq 25 \\ \qquad 3 \leq x_4 \leq 7,\ 7 \leq x_5 \leq 12 \end{cases} \tag{17}$$

where, $\boldsymbol{x}$ is a five-dimensional column vector with the L/D ratio, bowl speed, flow rate, differential speed, and half conical angle. $f(x)$ is the specific power, and $g(x)$ is the cake solid content. Both can be obtained by the results of the orthogonal numerical tests.

GAs (genetic algorithms) are considered one of the most widely used artificial intelligence techniques for effective search and optimization [22]. They are stochastic searching algorithms based on the mechanisms of natural selection and genetics. A GA program coded by MATLAB software is used based on the quadratic response surface regression model of the orthogonal test results. The minimum value of the cake solid content, $\alpha_{s,\min}$, is set to 72%. The parameters for the GA are shown in Table 3. The algorithm process is illustrated in Figure 4 and relevant details are given below:

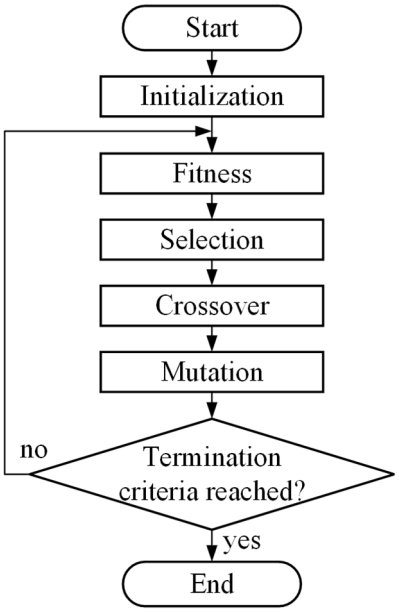

Figure 4. Flow chart of the genetic algorithm.

Step 1: Initialization. Randomly generate a certain number of chromosomes as a population.

Step 2: Fitness. A rank-based fitness assignment is adopted for further selection. As shown in Equation (17), there are two objective function values including the specific power and the L/D ratio. Their minimal values are preferred, so the fitness values are evaluated according to a descending rank of the objective function values. The minimal requirement of the cake solid content has to be satisfied, or the individual is not allowed to be selected. Thus, for individuals who fail to reach the condition of $g(x)$, the fitness value is set to zero. The fitness values are calculated as:

$$\text{Fitness} = \begin{cases} 2 - \varepsilon + 2 \times (\varepsilon - 1) \times \frac{N_i - 1}{N - 1}, & g(x) \geq \alpha_{s,\min} \\ 0, & g(x) < \alpha_{s,\min} \end{cases} \quad (18)$$

where N is the population size, and N_i is the individual rank in the population based on two objective function values. ε is the evaluation coefficient within the region [1.1, 2.0], which can affect the convergence time, and is taken at 1.1 in this study. It can be found that the fitness values are limited in the scope from 0.8 to 1.1, which means the superior individual cannot dominate extremely in the next selection to prevent premature convergence. The fitness value will increase when the rank of the individual rises, which also means the objective function values decrease since the rank is descending.

Step 3: Selection, crossover, and mutation. The roulette wheel selection method is chosen here. In this way, the fitness values of all individuals are represented by a pie chart. Each in the population is assigned a piece in the pie chart, and its size is proportional to its fitness value. Then, the wheel is rotated until the roulette stops. The pointer stops on one piece and the corresponding individual is selected. The higher the fitness value, the greater the possibility of being selected. The new individual is obtained by crossover from the gene segments of both its parents. All the factors are concatenated and encoded into a binary Gray code in the initialization step, so that parents can exchange genes from different regions to produce new individuals. Subsequently, new offspring arise after a random substitution of genes during mutation, which represents some original gene values at different regions in the coding string of the individual being replaced by random numbers with a small probability. Place new offspring as a new population and use this population for the next iteration.

Step 4: Circulation and end. When the maximum number of iterations is exceeded, the program ends.

Table 3. Parameters for the genetic algorithm.

Parameter	Value
Population size	60
Generation number	60
Probability of crossover	0.9
Probability of mutation	0.7

4. Results and Discussion

4.1. Flow Field Analysis

Figures 5 and 6 show the pressure distribution at the axis cross section (y = 0 mm) and in the radial direction, respectively. x_r is the radial distance to the central axis. The pressure consists of the static pressure and the pressure due to the rotating domain. As seen from the two figures, the pressure increases rapidly along the radius direction due to the centrifugal force. The pressure near the bowl at the junction of the cylindrical and conical sections is the highest in the whole field.

Figure 7 shows the velocity distribution along the radial direction at x = 500 mm and y = 0 mm. As can be seen from the figure, a tangential velocity lag exists compared with the ideal value, which is the product of angular velocity and bowl radius. This is unavoidable since the feed fails to be fully accelerated to the bowl speed in the feed accelerator. The lag is large at the bowl wall and small at the conveyor shaft wall. It can affect the centrifugal force on the particles as well as their settling rate.

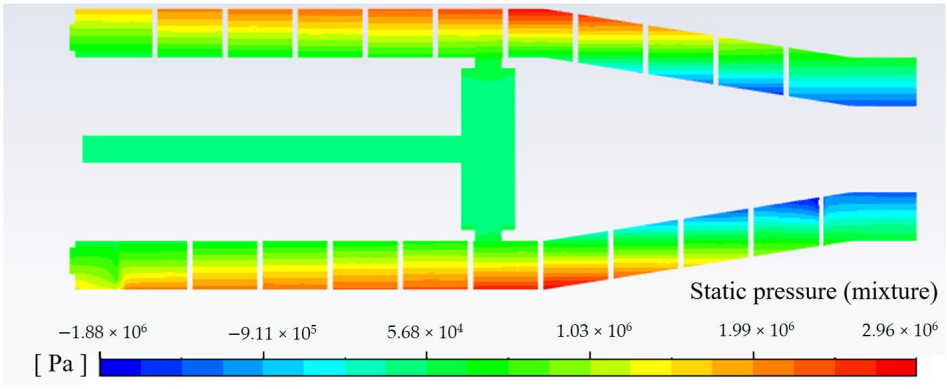

Figure 5. Pressure distribution at the axis cross section.

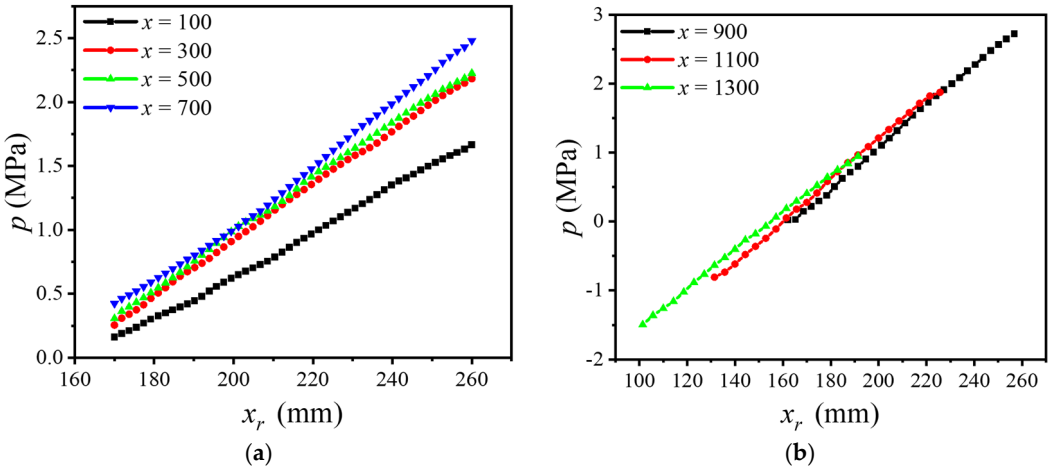

Figure 6. Pressure distribution in the radial direction. (**a**) Cylindrical section and (**b**) conical section.

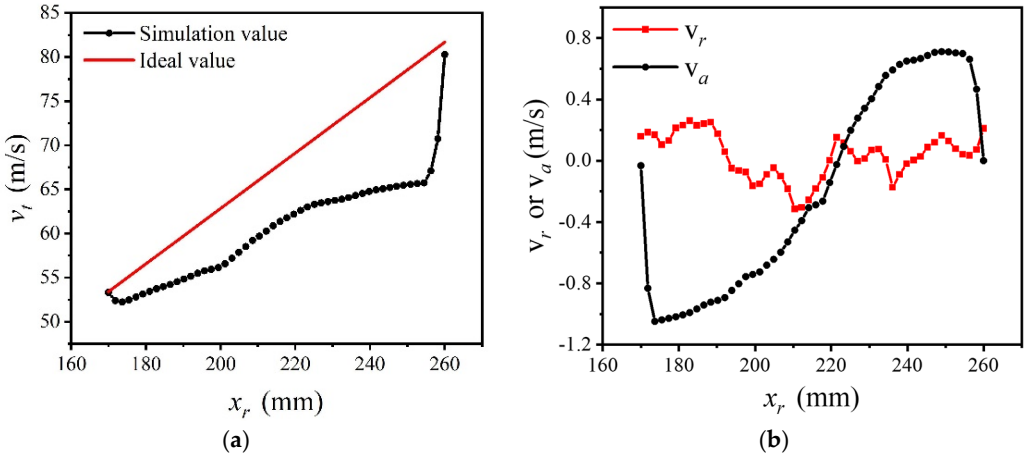

Figure 7. Velocity distribution along the radial direction at x = 500 mm and y = 0 mm. (**a**) Tangential velocity and (**b**) axial and radial velocity.

The axial velocity in the lower layer near the bowl is positive, because the cake is conveyed to the outlet by the screw conveyor. The axial velocity in the upper layer is negative, which indicates that the centrate flows to the opposite outlet. The radial velocity distribution has no obvious pattern. This mainly results from turbulence disturbance, which may refloat the separated particles and hinder the separation process.

4.2. Influence of a Single Parameter on the Separation Performance

According to Sigma theory [23–25], the separation performance can be improved by increasing the bowl diameter, rotary speed, and L/D ratio, which has been proven by the simulation [2,3]. Similarly, the influences of solid particle size and suspension viscosity were also investigated, which is in good agreement with Stokes' law. Thus, it is unnecessary to repeatedly investigate them in this paper.

4.2.1. Influence of the Gap between Bowl and the Screw Conveyor

The gap between the bowl and screw conveyor might be enlarged if wearproof measures at the blade edge are not applied or damaged. If the sediment fails to block the gap, a short circuit will occur. This means that some particles flow through the gap directly and further accumulate at the end of the cylindrical section.

The presence of the gap results in an adverse effect on the separation performance. Figure 8 shows the solid content distribution with and without the gap. Without the gap, the solid recovery and cake solid content are 99.98% and 71.49%, respectively. When the gap is 2 mm, both of them decline to 62.50% and 64.93%. Figure 8b shows that there is a solid retention zone at the rear of the bowl. This decreases the centrate clarity and solid recovery.

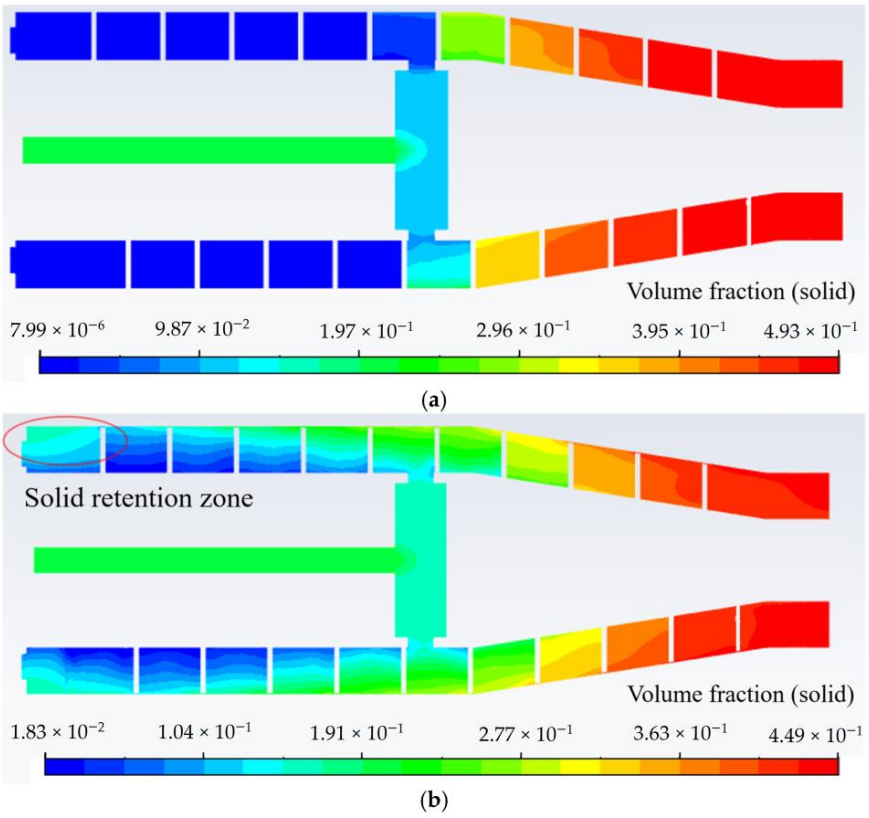

Figure 8. Solid content distribution with and without a gap: (**a**) 0 mm gap and (**b**) 2 mm gap.

4.2.2. Influence of Window Structure

The window refers to the holes on the conveyor or blade. When the window angle varies from 0 to 60° and the window height varies from 0 to 45 mm, the solid content distribution and the separation performance are investigated, as shown in Figures 9 and 10. The results demonstrate that the solid recovery and cake solid content decline with an increase in the window angle and height. Without the window structure, suspension can pass through the spiral flow channel to the outlet. This means that suspension has more residence time in the bowl for separation. Thus, it can be inferred that the window structure

facilitates the quick flow of the upper centrate to the outlet and results in less residence time for separation.

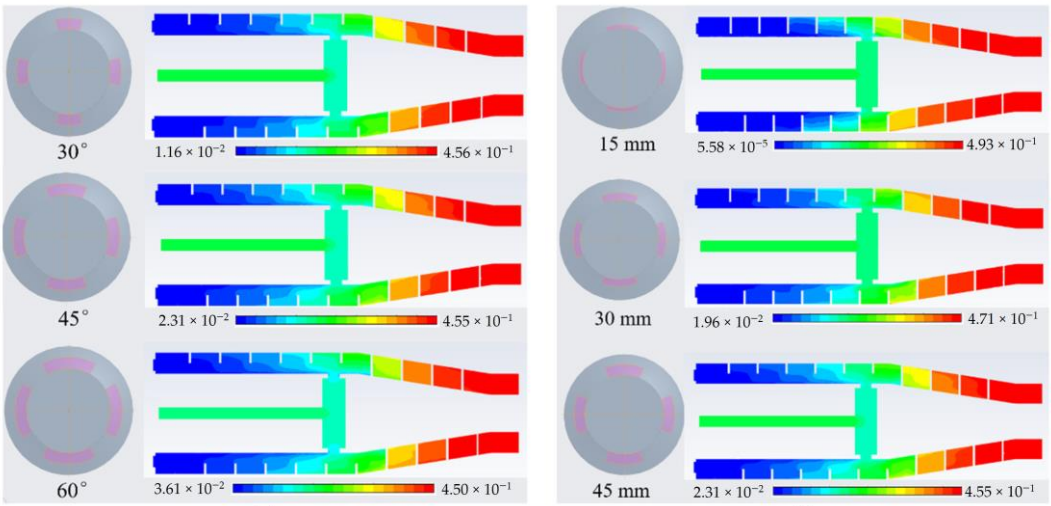

Figure 9. Solid content distribution at different window angles and heights. (**a**) Window angle and (**b**) window height.

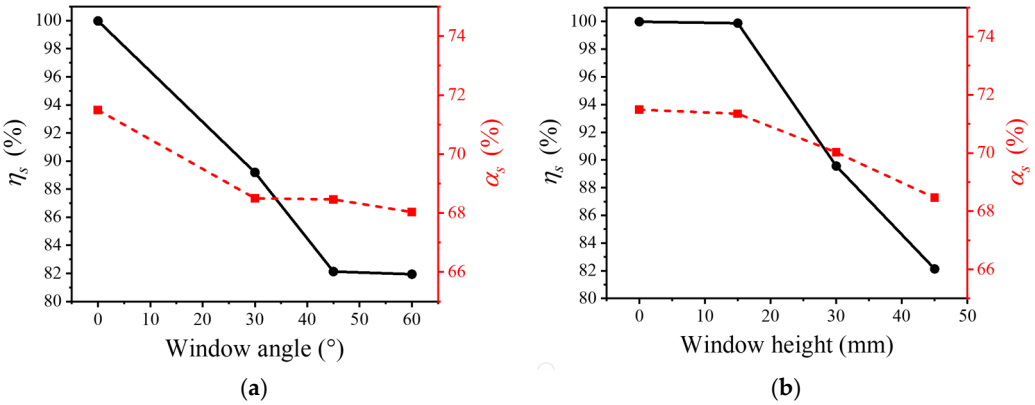

Figure 10. Separation performance at different window angles and heights. (**a**) Window angle (**b**) and window height.

To validate this speculation, the axial velocity distribution in the radial direction at x = 500 mm and y = 0 mm for three models is shown in Figure 11. For the model with a window, the velocity near the bowl is positive and modestly greater than that of the other two, but the velocity in the upper layer is much greater than that of the other two. For the model with a gap, the velocity near the bowl is negative. Both of them can deteriorate the separation performance, in agreement with the results.

4.3. Comprehensive Performance Optimization

4.3.1. Orthogonal Numerical Test Results

The results of the orthogonal numerical tests are shown in Figure 12. Bubble color represents the bowl speed, and bubble size represents the flow rate. Generally, the scheme with a better separation effect consumes more energy. The range, R, of each factor shows their significance levels on the separation performance: bowl speed (6.72) > flow rate (1.24) > differential speed (1.10) > half conical angle (0.76) > L/D ratio (0.61). The results show that the optimal scheme in terms of the cake solid content is $A_5B_5C_2D_1E_2$. The capital letters correspond to five factors in sequence, which are L/D ratio, bowl speed, differential

speed, flow rate, and half conical angle. The subscripts represent their levels, shown in Table 2. Furthermore, the significance levels for factors on the power consumption are obtained as follows: bowl speed (27.52) > flow rate (7.24) > differential speed (6.37) > L/D ratio (3.27) > half conical angle (1.99).

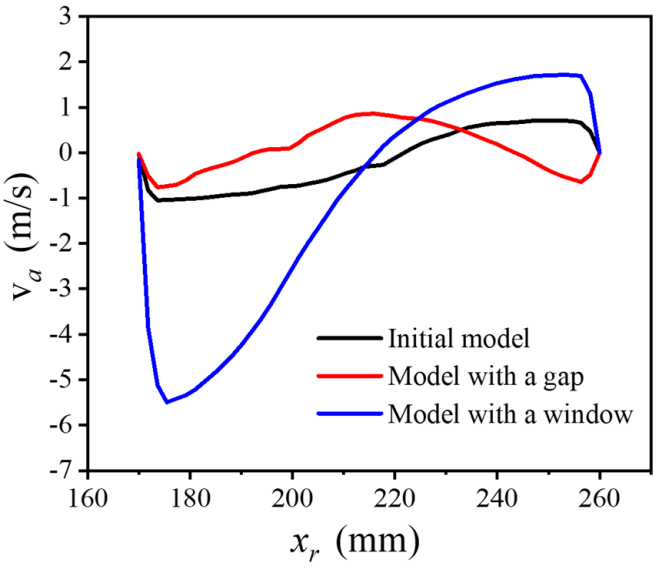

Figure 11. Axial velocity distribution in the radial direction at x = 500 mm and y = 0 mm for the three models.

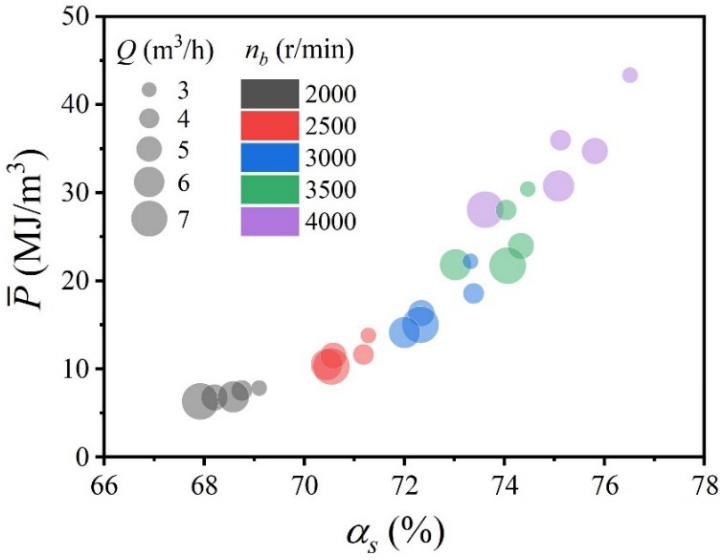

Figure 12. Results of the orthogonal numerical tests.

Figure 13 shows the influences of these factors on separation performance and power consumption. Generally, the cake solid content and specific power increase as the bowl speed increases, the L/D ratio increases, or the flow rate declines. For the geometrical model in this paper, the separation performance is optimal at a differential speed of 10 r/min and a half conical angle of 8°. There is a 95% confidence level at which the variation in the orthogonal test metrics is correlated with these five factors, which means that the error interference is excluded.

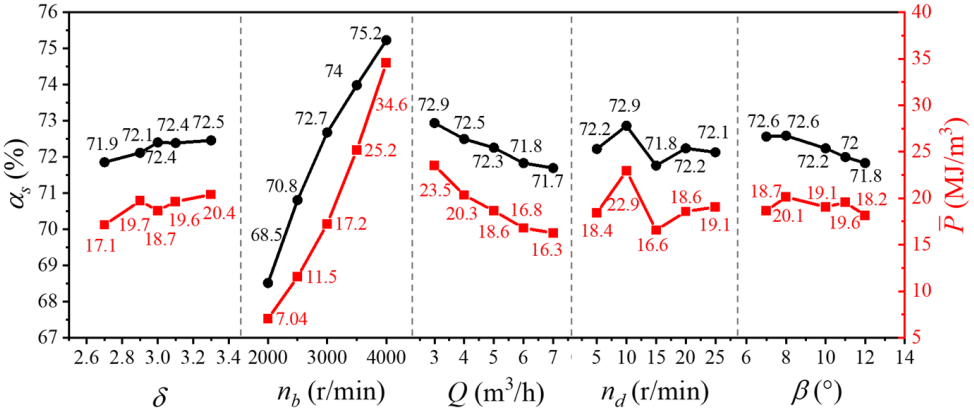

Figure 13. Influence of factors on separation performance and power consumption.

4.3.2. Results of Comprehensive Performance Optimization

Based on the results of the orthogonal tests, regression models of the cake solid content and specific power are obtained as the objective function for GA optimization.

$$\begin{aligned}\overline{P} = \; & -62.2 + 41.2\delta - 7.12 \times 10^{-3} n_b + 0.279 n_d \\ & -5.49Q + 3.81\beta - 6.05\delta^2 + 3.48 \times 10^{-6} {n_b}^2 \\ & -9.01 \times 10^{-3} {n_d}^2 + 0.367Q^2 - 0.208\beta^2\end{aligned} \tag{19}$$

$$\begin{aligned}\alpha_{s,out} = \; & 38.1 + 12.1\delta + 7.89 \times 10^{-3} n_b + 0.0256 n_d \\ & -0.620Q + 0.246\beta - 1.84\delta^2 - 7.61 \times 10^{-7} {n_b}^2 \\ & -1.09 \times 10^{-3} {n_d}^2 + 0.0305Q^2 - 0.0214\beta^2\end{aligned} \tag{20}$$

The optimization results of the genetic algorithm are shown in Figure 14 and Table 4. In the last generation, the specific power consumption of the optimized scheme is 11.82 MJ/m^3, while the cake solid content is 72%. Compared with the minimal specific power in the first generation, the optimized specific power is reduced by 15.7%. Accordingly, the L/D ratio is 2.87, the bowl speed is 2838 r/min, the differential speed is 5.0 r/min, the flow rate is 6.01 m^3/h, and the half conical angle is 7.0°.

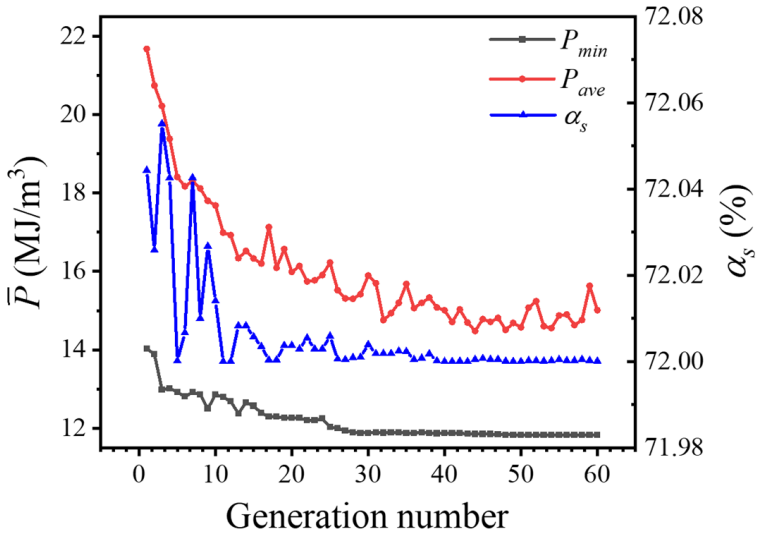

Figure 14. Optimization process of the genetic algorithm.

Table 4. Optimization results of the genetic algorithm.

Parameter	Range	Initial Value	Optimized Value
δ	[2.7, 3.3]	3.0501	2.8737
n_b (r/min)	[2000, 4000]	2781.2	2838.2
n_d (r/min)	[5, 25]	8.9325	5.0325
Q (m^3/h)	[3, 7]	5.5663	6.0139
β (°)	[7, 12]	8.3102	7.0009
α_s (%)	-	72.055	72.000
$\overline{P}$ (MJ/m^3)	-	14.027	11.824

5. Conclusions

In this paper, the influences of the window structure and bowl–conveyor gap on the separation performance of decanter centrifuges are analyzed by numerical simulation. A genetic algorithm-based method for optimizing the comprehensive performance of decanter centrifuges is proposed. An orthogonal numerical test is performed to obtain the regression models of cake solid content and specific power, which can be treated as the objective function for optimization. After systematic structural and parameter optimization, the optimal structural parameters of the decanter centrifuge studied in this paper are obtained. The main conclusions of this paper are as follows:

(1) The pressure near the bowl at the junction of the cylindrical and conical sections is the highest in the whole field. The lag of tangential velocity is large at the bowl wall and small at the conveyor shaft wall, which will affect the centrifugal force on the particles, as well as their settling rate.

(2) When the bowl–conveyor gap increases from 0 mm to 2 mm, both the solid recovery and cake solid content decrease by 37.5% and 6.6%, respectively. With an increase in the window angle from 0° to 60°, the solid recovery and cake solid content decrease by 17.9% and 3.0%, respectively. With an increase in the window height from 0 mm to 45 mm, the solid recovery and cake solid content decrease by 18.0% and 3.5%, respectively.

(3) Parameter optimization shows that the bowl speed and feed flow rate have the most significant effects on the separation performance and power consumption. Compared with the minimal specific power in the first generation, the optimized specific power is reduced by 15.7%, and the cake solid content merely decreases by 0.044%.

The results of this paper and the optimization method proposed in this paper can provide a technical basis for the design of an efficient and economical decanter centrifuge.

Moreover, although the orthogonal numerical test can be utilized for parameter optimization, it may cost a long calculation time under the restriction of calculation resources. Further studies will focus on the fast optimization method combined with artificial intelligence (AI) technology in the optimization process of decanter centrifuge structure.

Author Contributions: X.K.: methodology, investigation, and writing-original draft; L.C.: methodology, writing—reviewing and editing, and funding acquisition; Y.L.: supervision and Resources; X.G.: investigation and methodology; G.B.: investigation. All authors have read and agreed to the published version of the manuscript.

Funding: This research was funded by China Postdoctoral Science Foundation (No. 2020M680157) and the Fundamental Research Fund of the Central Universities (No. sxxj032020009).

Institutional Review Board Statement: Not applicable.

Informed Consent Statement: Not applicable.

Data Availability Statement: The authors confirm that the data supporting the findings of this study are available within the article and the referenced article.

Acknowledgments: The authors would like to thank the China Postdoctoral Science Foundation (No. 2020M680157) and the Fundamental Research Fund of the Central Universities (No. sxxj032020009) for funding.

Conflicts of Interest: The authors declare no conflict of interest.

Nomenclature

D	bowl diameter, mm
L	bowl length, mm
l_1	cylindrical section length, mm
l_2	conical section length, mm
h	pool depth, mm
β	half conical angle, °
$\dot{m}_f$	mass flow rate of the feed, kg/s
$\dot{m}_l$	mass flow rate at the centrate outlet, kg/s
$\dot{m}_s$	mass flow rate at the cake outlet, kg/s
n_b	bowl speed, r/min
n_d	differential speed, r/min
P	aggregate power, kW
P_A	feed acceleration power, kW
$\overline{P}$	specific power, MJ/m^3
Q	volume flow rate of the feed, m^3/h
R	bowl radius at the cylindrical section, mm
R_l	weir radius at the centrate outlet, mm
R_s	bowl radius at the cake outlet, mm
S	helical pitch of screw conveyor, mm
$\alpha_{l,feed}$	feed liquid content
$\alpha_{l,cake}$	cake liquid content
$\alpha_{l,cen}$	centrate liquid content
α_s	solid content
η_s	solid recovery
ω	angular velocity of the bowl, rad/s
δ	length to diameter (L/D) ratio

References

1. Records, A. *Decanter Centrifuge Handbook*; Elsevier: Amsterdam, The Netherlands, 2001.
2. Wu, L.; Qiu, F. Numerical simulation of the influence of the ratio of length to diameter on internal flow field of horizontal settling centrifuge. *Environ. Eng.* **2012**, 477–480.
3. Spelter, L.E.; Schirner, J.; Nirschl, H. A novel approach for determining the flow patterns in centrifuges by means of Laser-Doppler-Anemometry. *Chem. Eng. Sci.* **2011**, *66*, 4020–4028. [CrossRef]
4. Dong, L.; Shuangcheng, F.U.; Yuan, H. Numerical simulation on pressure field in a decanter centrifuge. *Chem. Ind. Eng. Prog.* **2014**, *33*, 309–336.
5. Fu, S.; Dong, L.; Yuan, H. Numerical simulation and analysis on flow field in a decanter centrifuge based on the Euler model. *Chem. Ind. Eng. Prog.* **2014**, *33*, 36–42.
6. Dong, L.D.; Yuan, H.X.; Fu, S.C.; Zou, X. Analysis on the Applicability of Turbulence Models for the Numerical Simulation of the Flow Field in a Decanter Centrifuge. *Fluid Mach.* **2013**, *10*, 25–29. [CrossRef]
7. Zhu, M.; Hu, D.; Xu, Y.; Zhao, S. Design and Computational Fluid Dynamics Analysis of a Three-Phase Decanter Centrifuge for Oil-Water-Solid Separation. *Chem. Eng. Technol.* **2020**, *43*, 1005–1015. [CrossRef]
8. Zhu, G.; Zhang, A.; Peng, N.; Ba, S.; Chen, Y.; Hu, Z. CFD-PBM coupled calculation on salt-out flow field in decanter centrifuge. *Chem. Ind. Eng. Prog.* **2019**, *38*, 3947–3955.
9. Zhu, G.; Zhang, A.; Peng, N.; Ba, S.; He, W.; Hu, Z. Effect of drum rotational speed on flow field characteristics of decanter centrifuge for solid-liquid separation of salt sludge. *Chem. Ind. Eng. Prog.* **2019**, *38*, 2590–2599.
10. Romaní, X.; Fernández, H. Nirschl, Simulation of particles and sediment behaviour in centrifugal field by coupling CFD and DEM. *Chem. Eng. Sci.* **2013**, *94*, 7–19. [CrossRef]
11. Menesklou, P.; Nirschl, H.; Gleiss, M. Dewatering of finely dispersed calcium carbonate-water slurries in decanter centrifuges: About modelling of a dynamic simulation tool. *Sep. Purif. Technol.* **2020**, *251*, 117287. [CrossRef]
12. Gleiss, M.; Nirschl, H. Modeling Separation Processes in Decanter Centrifuges by Considering the Sediment Build-Up. *Chem. Eng. Technol.* **2015**, *38*, 1873–1882. [CrossRef]

13. Hammerich, S.; Gleiss, M.; Stickland, A.D.; Nirschl, H. A computationally-efficient method for modelling the transient consolidation behavior of saturated compressive particulate networks. *Sep. Purif. Technol.* **2019**, *220*, 222–230. [CrossRef]
14. Zhu, G.; Tan, W.; Yu, Y.; Liu, L. Experimental and Numerical Study of the Solid Concentration Distribution in a Horizontal Screw Decanter Centrifuge. *Ind. Eng. Chem. Res.* **2013**, *52*, 17249–17256. [CrossRef]
15. Yuan, H.; Zhang, Y.; Fu, S.; Jiang, Y. Influence of the Length-Diameter Ratio and the Depth of Liquid Pool in a Bowl on Separation Performance of a Decanter Centrifuge. In Proceedings of the Advanced Manufacturing and Automation VIII, Changzou, China, 20–21 September 2019; pp. 78–85. [CrossRef]
16. Zhou, C.; Ling, Y.; Shen, W.; Liu, M. Numerical Study on Sludge Dewatering by Horizontal Decanter Centrifuge. *J. Mech. Eng.* **2014**, *50*, 206–212. [CrossRef]
17. Gidaspow, D.; Bezburuah, R.; Ding, J. Hydrodynamics of Circulating Fluidized Beds: Kinetic Theory Approach. In Proceedings of the 7th International Conference on Fluidization, Gold Coast, Australia, 3–8 May 1992.
18. SOrszag, A.; Yakhot, V.; Flannery, W.; Boysan, F.; Choudhury, D.; Maruzewski, J.; Patel, B. Renormalization group modeling and turbulence simulations. In Proceedings of the International Conference on Near-Wall Turbulent Flows, Tempe, AZ, USA, 15–17 March 1993; pp. 1031–1046.
19. Bell, G.R.A. Analysis and Development of a Decanter Centrifuge: Power Consumption Analysis, Development of a Composite Bowl, and Feed Accelerator Analysis. Ph.D. Thesis, University of Canterbury, Christchurch, New Zealand, 2013.
20. Bell, G.; Symons, D.; Pearse, J. Mathematical model for solids transport power in a decanter centrifuge. *Chem. Eng. Sci.* **2014**, *107*, 114–122. [CrossRef]
21. Ling, Z.; Shi, W.; Wu, S. Performance Optimization in a Centrifugal Pump Impeller by Orthogonal Experiment and Numerical Simulation. *Adv. Mech. Eng.* **2013**, *5*, 385809.
22. Goldberg, D.E.; Holland, J.H. Genetic algorithms and machine learning. *Mach. Learn.* **1988**, *3*, 95–99. [CrossRef]
23. Ambler, C.M. Theory of centrifugation. *Ind. Eng. Chem.* **1961**, *53*, 430–433. [CrossRef]
24. Ambler, C.M. The evaluation of centrifuge performance. *Chem. Eng. Prog.* **1952**, *48*, 150–158.
25. Ambler, C.M. The theory of scaling up laboratory data for the sedimentation type centrifuge. *J. Biochem. Microbiol. Technol. Eng.* **1959**, *1*, 185–205. [CrossRef]